A diverse family of layered frustrated magnets with tailorable inter-layer interactions

Wenjiao Yao,[†] Lucy Clark,[§,] Mingjun Xia,[¶] Teng Li,[†] Stephen L. Lee,[‡] Philip Lightfoot,[†,*]

[†] School of Chemistry, University of St Andrews, St Andrews, Fife KY16 9ST, U.K.

[§] Departments of Chemistry and Physics, School of Physical Sciences, University of Liverpool, Liverpool, L69 7ZD, U.K.

[¶] Beijing Center for Crystal Research and Development, Key Laboratory of Functional Crystals and Laser Technology, Technical Institute of Physics and Chemistry, Chinese Academy of Sciences, Beijing 100190, China

[‡] School of Physics and Astronomy, University of St Andrews, St Andrews, Fife, KY16 9SS, U.K.

ABSTRACT: An extended family of iron oxalates, featuring two-dimensional, geometrically frustrated networks of kagome or triangular magnetic motifs with a range of structurally distinct inter-layer bridges, is obtained through the selective engineering of chemical bonding. The present work succinctly illustrates how both crystallographic and magnetic dimensionalities can be manipulated by chemical tuning, affording an unusual degree of control over the ensuing properties of the materials studied. Magnetic susceptibility measurements reveal strong antiferromagnetic correlations between the Fe^{2+} centres in one of the novel compounds presented here and a high degree of spin frustration resulting from the topology of the magnetic layers. There is also evidence for an intriguing competition of exchange interactions between inter-layer and intra-layer interactions resulting in quasi-one-dimensional magnetic behaviour.

Crystal structures composed of two-dimensional (2D) sheets of magnetic species arranged in triangular motifs are of great current interest for the understanding and exploitation of frustrated magnetism. The two distinct primary examples of triangle-based magnetic lattices are the triangular and kagome lattices, formed from networks of edge- and corner-sharing triangles of magnetic species, respectively.[1-7] Metal oxalates have attracted increasing attention for their magnetic properties in recent years.[8-15] The oxalate moiety has a great ability to provide either antiferromagnetic or ferromagnetic super-exchange pathways partly due to its wide variety of coordination modes between metal centres.[16] The relatively low melting point of oxalic acid (103.5 °C) and its self-flux property add further advantage of mild synthesis conditions to the exploration of novel oxalates.[17] The magnetic properties of many oxalate-based materials have been reported, formed from isolated clusters, 1D chains, 2D layers, or 3D networks of metal ion centres.[8-18]

During our previous investigations of metal-oxalate systems,[19-22] primarily to explore their potential as cathode materials in Li or Na ion batteries, we have observed that several hydrothermally-prepared oxalates are characterised by a 2D $[Fe(C_2O_4)]_\infty$ network, with a triangular arrangement of oxalate-bridged magnetic Fe^{2+} nodes. Examples include $(NH_4)_2Fe(C_2O_4)_2{\cdot}H_2O$ (***A***),[23] $K_4Na_2[Fe(C_2O_4)_2]_3{\cdot}3H_2O$ (***B***),[24] $K_2[Fe(C_2O_4)(HPO_4)(H_2O)]{\cdot}H_2O$ (***C***),[25] $Na_2Ba_3[Fe^{II}_3(C_2O_4)_6]$ $[A^{IV}(C_2O_4)_3]$ (A = Sn, Zr) and $Na_2Ba_3[Fe^{II}_3(C_2O_4)_6][A^{III}(C_2O_4)_3]_{0.5}[A^{III}(C_2O_4)_2]_{0.5}$ (A = Al, Fe) (***D***[§]).[26] In spite of the same chemical formula, $[Fe(C_2O_4)]_\infty$, we notice that there are actually two distinct polymorphic arrangements within the iron oxalate layers of this family of compounds. The crystal-chemical differences between these are discussed later, but significantly these give rise to two distinct types of magnetic sublattice, viz. a distorted kagome or distorted triangular sublattice,

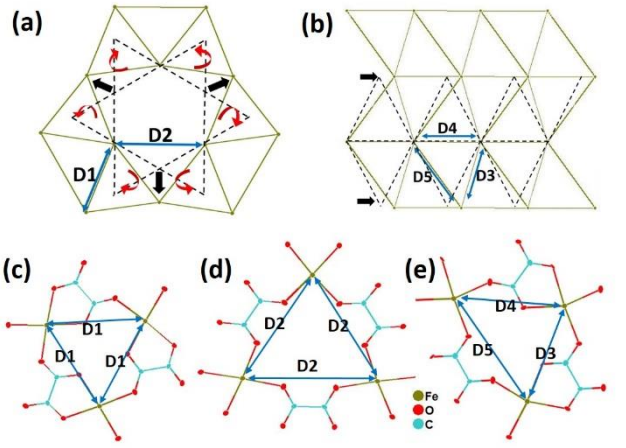

Figure 1. Magnetic sublattices observed in the planar $[Fe(C_2O_4)]_\infty$ networks. (a) *Type-1*, distorted kagome lattice, (b) *Type-2*, distorted triangular lattice. Dotted lines represent the ideal configuration, black arrows show lattice distortion, and red curved arrows show triangular rotation. D1-D5 highlight different magnetic interaction pathways in the distorted structures. Fe positions only are plotted for clarity. (c-e) Detailed connections in (a) and (b).

Table 1. Comparison of 2D $[Fe(C_2O_4)]_\infty$ lattice-containing compounds. Type 1/2, D1-D5 as indicated in Figure 1.

Compound	Space group	Bridge	D_{layers}(Å)	Type	D1-D5 (Å)
$(NH_4)_2Fe(C_2O_4)_2 \cdot H_2O$ (***A***)	*P*321	$(C_2O_4)^{2-}$	7.377(1)	1	5.496(2), 6.797(3)
$Na_2K_4(Fe(C_2O_4)_2)_3 \cdot 3H_2O$ (***B***)	*P*321	$(C_2O_4)^{2-}$	7.461(1)	1	5.503(1), 6.933(2)
$K_2Fe(C_2O_4)(HPO_4) \cdot H_2O$ (***C***)	*P*bca	none	7.668(5)	2	5.543(2), 5.953(1), 6.578(1)
$KFe(C_2O_4)F$ (***I***)	*C*mc2$_1$	F^-	3.890(2)	2	5.475(2), 5.920(2), 6.672(1)
$Li_2[Fe(C_2O_4)Cl_2][Fe(C_2O_4)(H_2O)_2] \cdot 2H_2O$ (***II***)	*P*ca2$_1$	none	5.583(2)	2	5.332(1), 5.727(1), 6.514(5) 5.351(2), 5.749(4), 6.493(1)
$Na_2Fe(C_2O_4)(SO_4) \cdot H_2O$ (***III***)	*P*-62m	$(SO_4)^{2-}$	6.487(4)	1	5.567(3), 6.921(4)

illustrated schematically in **Figure 1** (a-b), respectively. In addition, the $[Fe(C_2O_4)]_\infty$ layers in ***C*** stack in a different manner than in ***A*** and ***B***. It appears that these similarities and differences have not been noticed previously and, therefore, these systems provide a great opportunity to explore and extend the solid-state chemistry of frustrated and chemically-tunable magnets. In particular, we note that the 2D $[Fe(C_2O_4)]_\infty$ networks are apparently stable structural motif under various synthesis conditions. However, the inter-layer connectivity opens a route to further structural flexibility, based on the presence of additional linking and separating ions, such as halides, $(XO_4)^{n-}$ (X = P, S), and alkali metals. In this paper we report three novel additions to this family of frustrated magnets; each exhibits one of the polymorphic $[Fe(C_2O_4)]_\infty$ layers, but differs in the chemical nature of inter-layer linkage and separation of the layers. Systematic explorations were carried out in several related systems, each incorporating Fe^{2+} and oxalate ions together with further potential anionic linkers and charge-balancing cations. We successfully obtained three novel compounds, formulated as $KFe(C_2O_4)F$(***I***), $Li_2[Fe(C_2O_4)Cl_2][Fe(C_2O_4)(H_2O)_2] \cdot 2H_2O$ (***II***), and $Na_2Fe(C_2O_4)SO_4 \cdot H_2O$ (***III***). In addition to the 2D $[Fe(C_2O_4)]_\infty$ network, each displays a distinct inter-layer bridging mode, *viz*. a single ion (F^-) bridge in ***I***, a complex anion $(SO_4)^{2-}$ bridge in ***III*** and no direct covalent bridge in ***II***.

Crystals of ***I***, ***II***, and ***III*** were prepared by hydrothermal synthesis in a Teflon-lined autoclave, and crystal structures were determined using single crystal X-ray diffraction (XRD). Full details of the synthesis and characterisation are given in Supporting Information (*SI*). More detailed structural information and views of each of the compounds ***I*** – ***III*** are given in the *SI* (Table S1 and Figure S1). Figure 1 (c-e) show differing building units of the distinct $[Fe(C_2O_4)]_\infty$ layer topologies common to each type of the compounds. A comparison of structural and crystallographic features for the whole family is provided in **Table 1**.

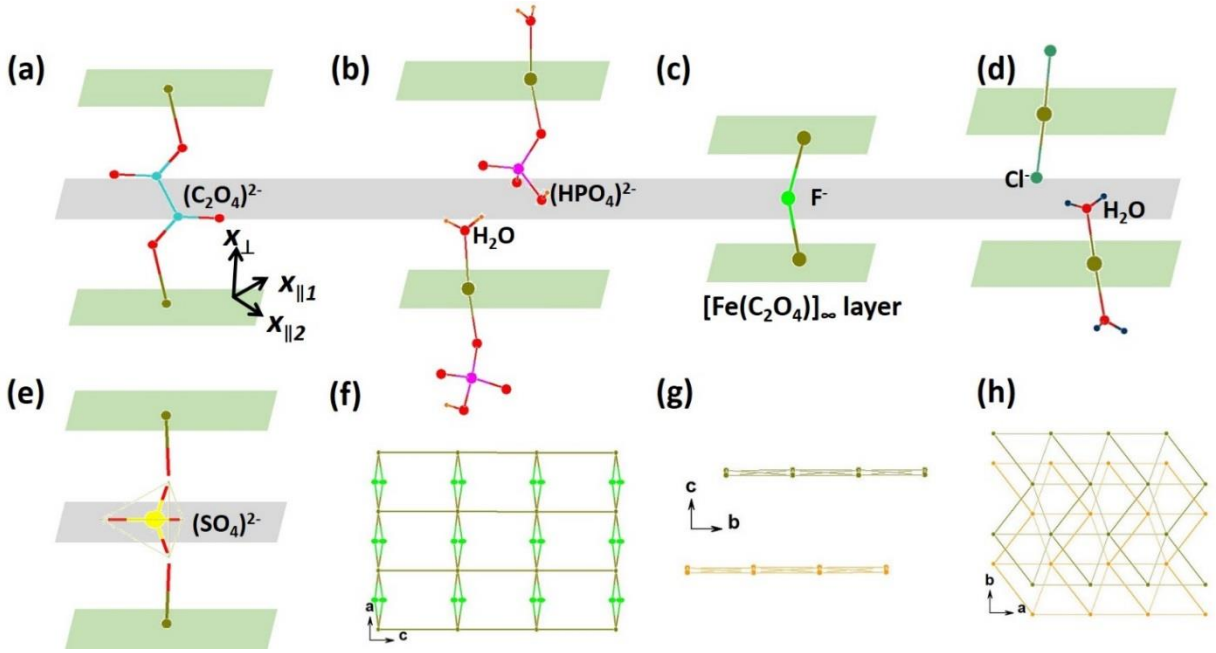

Figure 2. A representation of layered iron oxalates. Layers connected by (a) a trans-oxalate, as in ***A***, (b) without covalent connection, as in ***C***, (c) a single F^- ion, as in ***I***, (d) without covalent connection, as in ***II***, (e) an $(SO_4)^{2-}$ tetrahedron, as in ***III***. (f) Eclipsed layers in ***I***. (g-h) Staggered layers in ***C***. The $[Fe(C_2O_4)]$ motif in (a) and (e) belongs to *type-1* (D_{3h} symmetry), while the bridging oxalate breaks $m_\perp$ as well as three $m_\parallel$. This leaves only C_3 and C_2 symmetry, as indicated by their space group *P*321. However, the replacement of tetrahedral sulphate for the pillaring oxalate as in (b) retains all mirror planes and adds an additional *m* in the *c*-axis, hence the space group changes from *P*321 to $P\bar{6}2m$. This clearly shows that the overall symmetry is manipulated by the bridge. Cations and free water molecules are omitted for clarity.

When comparing the significant magnetic interaction pathways of the newly discovered compounds, in comparison with those previously known, examples of the two different aforementioned network types are observed. The "*type-1*" network consists of two types of iron oxalate building block based on equilateral triangle motifs (Figure 1 c-d). The two triangles differ in the mode of connectivity of the Fe nodes *via* the oxalate ligands, the smaller triangle (edges D1) having Fe-O-C-O-Fe connectivity with oxalate ligands connected in a *syn-anti* way. The larger triangle (edges D2) has Fe-O-C-C-O-Fe connectivity with oxalate ligands bridging in *cis* manner. Overall, the *type-1* network retains 3-fold symmetry. The "*type-2*" network is built from one type of scalene triangle, with the lower symmetry caused by mixed bridging modes (*syn-anti* and *cis*) of the oxalates groups. As shown in Table 1, the distorted kagome lattice (*type-1*) occurs in compounds ***A***, ***B*** and ***III***, whereas the distorted triangular lattice (*type-2*) is shared by compounds ***I***, ***II*** and ***C***. In the *type-1* variant, the smaller triangle (edge-length D1) are expected to give rise to the strongest in-plane magnetic exchanges pathways, but the longer D2 pathways may also provide a significant interaction. D2 is typically around 1.3 Å larger than D1. Lhotel *et al.* have reported the magnetic properties of this *type-1* lattice based on compounds ***D***, which exhibited an antiferromagnetic spin-order below the Néel temperature with exchange and dipolar interactions, and multiaxial anisotropy.[26] The *type-2* distortion results in a lateral "slanting" of a regular triangular lattice, as displayed in Figure 1(b). The oxalate connectivity effectively compresses one triangular side (D3), extends the second (D5), and keeps the third unchanged (D4), in comparison with the ideal equilateral triangular lattice. Therefore, the derived M-M distances follow the sequence D3 < D4 < D5. In compounds ***I***, ***II*** and ***C***, D3 and D4 correspond to O-C-O connection modes, and D5 to an O-C-C-O mode. Intra-layer metal-metal distances for both types are listed in Table 1.

Table 1 also compares inter-layer connections in this family of compounds, D_{layers}. It can be seen that the $[Fe(C_2O_4)]_\infty$ networks in ***A***, ***B***, ***I*** and ***III*** are linked directly by bridging groups and therefore form 3D frameworks, whereas those in ***C*** and ***II*** are isolated and thus feature 2D frameworks, with no direct covalent links. The inter-layer distance in the 3D structures follows the sequence ***I*** < ***III*** < ***A***, ***B***, which corresponds to the size of the bridging ligand. The $[Fe(C_2O_4)]_\infty$ layers are stacked in an eclipsed manner in the perpendicular direction, and the resultant lowering of space group symmetry arises from the symmetry of the bridging ligand, as shown schematically in **Figure 2**.

Structures of the *type-2* compounds ***I***, ***II*** and ***C*** are more complex. The distortion of the 2D $[Fe(C_2O_4)]_\infty$ network lowers the overall symmetry from trigonal/hexagonal to orthorhombic. In compound ***C***, identical $[Fe(C_2O_4)]_\infty$ layers lie in the *ab* plane but the H_2O and HPO_4 moieties act as terminal, rather than bridging, ligands on each side of the layer. In ***I*** and ***II***, the iron-centred octahedra are completed by the same atoms or ions (F^-, Cl^-, or H_2O). The *type-2* layer itself is polar, but in compound ***C***, neighbouring polar layers align in opposite directions, resulting in a nonpolar structure, while the layers in ***I*** or ***II*** point in the same direction, resulting in polar (2_1) symmetry. (Figure S5)

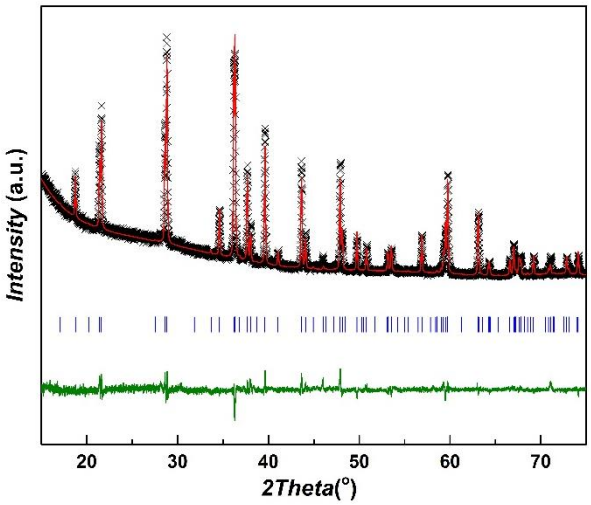

Figure 3. Rietveld fit of powder XRD for sample ***I*** at room temperature; $Cmc2_1$ space group, a = 7.7802 (1) Å, b = 11.8831(2) Å, c = 10.4216(2) Å, wR_p=0.0647, R_p=0.048, χ^2=1.772.

Another facet worth pointing out is the different mode of layer-stacking displayed by bridged and non-bridged variants. As shown in Figure 2 (f-h), the $[Fe(C_2O_4)]_\infty$ layers in the 3D frameworks are all fully overlapped, while in the 2D frameworks they are packed in a staggered way. We posit that the adjacent layers are inherently inclined to misalign with each other to minimise repulsions, but the introduction of pillars stabilises the eclipsed stacking.

Preliminary magnetic measurements on ***I*** reveal some interesting magnetic behaviour. The purity of a polycrystalline sample of ***I*** was confirmed by Rietveld analysis of powder XRD data (Figure 3). Figure 4(a) shows the temperature dependences of the magnetic and inverse susceptibilities of polycrystalline ***I*** measured in a zero-field- cooled (ZFC) field-cooled (FC) cycle over 2 – 300 K. Above 100 K, the system can be modelled as a Curie-Weiss magnet. Curie-Weiss fitting of the high temperature inverse susceptibility data indicates strong, dominant antiferromagnetic exchange interactions with a Weiss constant, θ = −301(2) K, and an effective paramagnetic moment typical of that observed for high-spin Fe^{2+}. Below T_c ~ 20 K, the system appears to undergo a long-range magnetic ordering transition. Comparing the energy scale for magnetic order in ***I*** with the energy scale for magnetic exchange set by the Weiss constant, $|\theta|/T_c$ ~ 15, suggests that spin order in the system is highly frustrated. Interestingly, the magnetic susceptibility data for ***I*** also reveal a broad maximum centred ~ 100 K (Figure 4(b)) that may indicate the onset of short-range magnetic correlations above the ordering transitions. Indeed, this broad feature can be very well described in by a 1D spin chain model, yielding an intra-chain coupling constant J = 8.46(4) K (see *SI*). This suggests that the magnetic sublattice in ***I*** undergoes a one- to three-dimensional crossover upon cooling that stems from the different magnetic exchange pathways within its layered structure.

From the present data it cannot be determined whether the 1D magnetic behaviour at higher temperature corresponds to the short Fe-F-Fe inter-layer pathways (Fe---Fe ~ 3.89 Å) or to a more complex intra-layer pathway: the shortest intra-layer pathway arises from chains of oxalate-bridged Fe---Fe along the *c*-axis *via* D3. This apparent competition of exchange interactions *via* the fluoride and oxalate anions in ***I*** is an intriguing phenomenon and one that is currently under further investigation. Moreover, the ability to tailor both the $[Fe(C_2O_4)]_\infty$ network type and the nature of inter-layer interactions suggests a much richer range of magnetic behaviours is likely within this family.

In addition to their interesting magnetic properties, these novel compounds are noteworthy in several other regards. A promising avenue of research is to explore their electrochemical performance as battery materials since their structures possess large channels for alkali metals (either K^+, Na^+, or Li^+) to migrate and the valence state of Fe is adjustable. In particular, ***I*** displays a robust 3D framework stable up to 300 °C as indicated by thermogravimetric analysis, and large channels in the [100], [010], and [013] directions (Figure S6). Moreover, its theoretical capacity (140 mAh/g) is comparable to the commercial cathode material $LiFePO_4$. These new materials also hold promise for nonlinear optical and multiferroic behaviour due to the inherent polar and/or noncentrosymmetric structures. For structural chemists, the reported compounds will also inspire the discovery of new families of compounds using other compositional variants. For example, we have so far successfully obtained $A^+M^{2+}(C_2O_4)F$ (for K-Mn/Co, Rb-Fe/Co and NH_4-Fe combinations), all displaying the same 3D framework as their K-Fe counterpart.

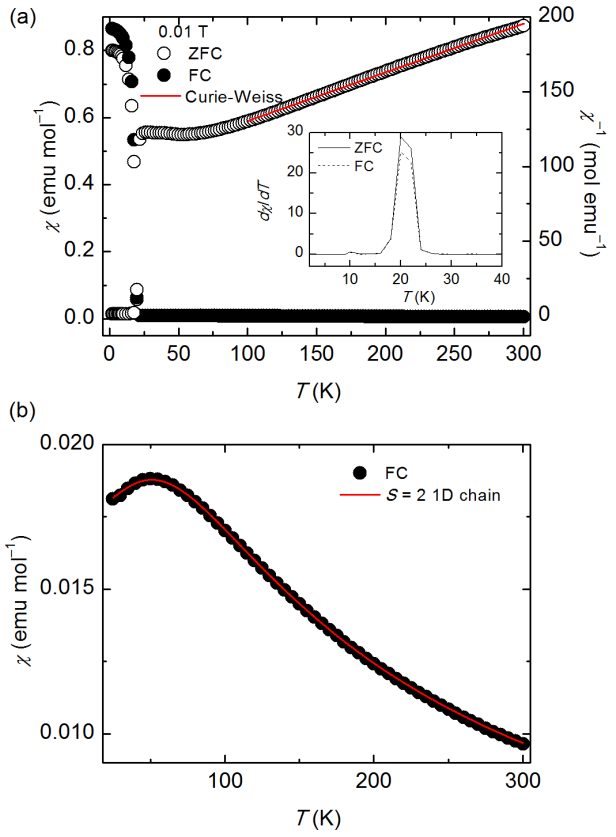

Figure 4. Temperature-dependent magnetic susceptibility of ***I***, from 2 to 300 K. (a) Data above 100 K (0.01 T external field) are modelled according to the Curie-Weiss law (solid red line) with $\theta = -301(2)$ K, $\mu_{eff} \sim 5.5\ \mu_B$ per Fe^{2+}. Taking the derivative of the magnetic susceptibility (inset) clearly reveals a magnetic ordering transition at T ~ 20 K. (b) Detailed magnetic susceptibility around 100 K. Solid red line is the modelled curve according to an $S = 2$ one-dimensional chain model with an intra-chain coupling $J = 8.46(4)$ K.

In conclusion, the present work demonstrates that the inter-layer linkage is a chemical-bonding weakness in layered oxalates and illustrates a successful route to new solid-state materials through the selective engineering of the weaker bond. It provides new insight into the controlled self-assembly of complex magnetic architectures from only a few known cases, and illustrates how both the magnetic and crystallographic dimensionality can be manipulated by chemical tuning. The realisation of the weakness in the structure not only offers the possibility of preparing materials with interesting properties, but also offers a way to target the synthesis of many new materials.

ASSOCIATED CONTENT

Supporting Information. Detailed experiment procedures, Fourier-transform infrared (FTIR) patterns, thermogravimetric analysis, crystal information file (CIF) are attached as the supporting files. This material is available free of charge via the Internet at http://pubs.acs.org.

AUTHOR INFORMATION

Corresponding Author

*pl@st-andrews.ac.uk (PL)

NOTES AND ACKNOWLEDGMENT

§ Crystal information files (cif) are not found in either ICSD or CSD. According to the original paper, family D is isostructural to A.

We acknowledge the Royal Society for the award of a Newton International Fellowship (140881) and Leverhulme Trust (RPG-2013-343). We thank Dr Khang Hoang from the Center for Computationally Assisted Science and Technology, North Dakota State University, Fargo, ND 58108, USA, and Jianing Hui from the School of Chemistry, University of St Andrews, UK, for helpful discussions. The manuscript was written through contributions of all authors. All authors have given approval to the final version of the manuscript.

REFERENCES

[1] B. Bemu, C. Lhuillier and L. Pierre. Signature of Néel order in exact spectra of quantum antiferromagnets on finite lattices. *Phys. Rev. Lett.*, **1992**, *69*, 2590-2593.

[2] M. P Shores, E. A. Nytko. B. M. Bartlett and D. G Nocera, A Structurally Perfect S = 1/2 Kagomé Antiferromagnet. *J. Am. Chem. Soc.*, **2005**, *127*, 13462-13463.

[3] J. S. Helton, K. Matan, M. P. Shores, E. A. Nytko, B. M. Bartlett, Y Yoshida, Y Takano, Y Qiu, J.H. Chung, D. G Nocera and Y

S. Lee, Spin Dynamics of the Spin-1/2 Kagome Lattice Antiferromagnet $ZnCu_3(OH)_6Cl_2$. *Phys. Rev. Lett.*, **2007**, *98*, 107204.

[4] S. K. Pati and C. N. R. Rao, Kagome network compounds and their novel magnetic properties. *Chem. Comm.*, **2008**, 4683-4693.

[5] K. M. Kojima, R. Kadono, M. Miyazaki, M. Hiraishi, I. Yamauchi, A. Koda, Y. Tsuchiya, H. S. Suzuki, and H. Kitazawa. Magnetic Frustration in Iridium Spinel Compound $CuIr_2S_4$. *Phys. Rev. Lett.*, **2014**, *112*, 087203.

[6] L. Clark, F. H. Aidoudi, C. Black, K. S. A. Arachchige, A. M. Z. Slawin, R. E. Morris, and P. Lightfoot. Extending the Family of V^{4+} S = 1/2 Kagome Antiferromagnets. *Angew. Chem. Int. Ed.*, **2015**, *54*, 15457-15461.

[7] F. D. Romero, M. J. Pitcher, C. I. Hiley, G. F. S. Whitehead, S. Kar, A. Y. Ganin, D. Antypov, C. Collins, M. S. Dyer, G. Klupp, R. H. Colman, K. Prassides and M. J. Rosseinsky, Redox-controlled potassium intercalation into two polyaromatic hydrocarbon solids. *Nature Chem.*, **2017**, *9*, 635-643.

[8] R. Pellaux, H. W. Schmalle, R. Huber, P. Fischer, T. Hauss, B. Ouladdiaf, and S. Decurtins, Molecular-Based Magnetism in Bimetallic Two-Dimensional Oxalate-Bridged Networks. An X-ray and Neutron Diffraction Study. *Inorg. Chem.* **1997,** *36,* 2301-2308.

[9] S. Decurtins, R. Pellaux, G. Antorrena and F. Palacio, Multifunctional coordination compounds: design and properties. *Coord. Chem. Rev.*, **1999**, *190-192*, 841-854.

[10] S. G. Carling and P. Day, A Monte Carlo study of honeycomb lattice ferrimagnets. *Polyhedron*, **2001**, *20*, 1525-1528.

[11] D. J. Price, S. Tripp, A. K. Powell, and P. T. Wood. Hydrothermal Synthesis, X-Ray Structure and Complex Magnetic behaviour of $Ba_4(C_2O_4)Cl_2[\{Fe(C_2O_4)(OH)\}_4]$. *Chem. Eur. J.* **2001**, *7* (1), 200-208.

[12] M. B. Hursthouse, M. E. Light and D. J. Price. One-Dimensional Magnetism in Anhydrous Iron and Cobalt Ternary Oxalates with Rare Trigonal- Prismatic Metal Coordination Environment. *Angew. Chem. Int. Ed.* **2004**, *43*, 472-475.

[13] B. L. Fei, R. Clerac, C. E. Anson and A. K. Powell. Crystal structure and magnetic properties of a *pseudo*-cubic close-packed array of oxalate linked $\{Fe^{II}_6(\mu\text{-}OH)_6\}^{6+}$ clusters. *Dalton Trans.*, **2005**, 1381-1386.

[14] H Yamaguchi, Y Nakagawa, T Kashiwagi, S Kimura, Z Honda, K Kindo and M Hagiwara. High field magnetization and multi-frequency ESR in the spin-ladder compound $Na_2Fe_2(C_2O_4)_3(H_2O)_2$. *J. Phys.: Conference Series*, **2006**, *51*, 191-194.

[15] G. Rousse and J. Rodríguez-Carvajal. Oxalate-mediated long-range antiferromagnetism order in $Fe_2(C_2O_4)_3{\cdot}4H_2O$. *Dalton Trans.*, **2016**, *45*, 14311-14319.

[16] J. S. Miller, M. Drillon. Magnetism: Molecules to Materials II: molecule based materials. Wiley-VCH Verlag Gmbh & Co. GaA. ISBN: 3-527-30301-4.

[17] D. Abeysinghe, M. D. Smith, J. Yeon, G. Morrison and H. C. Z. Loye, Observation of Multiple Crystal-to-Crystal Transitions in a New Reduced Vanadium Oxalate Hybrid Material, $Ba_3[(VO)_2(C_2O_4)_5(H_2O)_6]{\cdot}(H_2O)_3$, Prepared via a Mild, Two-Step Hydrothermal Method. *Cryst. Growth Des.*, **2014**, *14*, 4749-4758.

[18] S. H. Yang, G. B. Li, S. J. Tian, F. H. Liao and J. H. Lin, *Eur. J. Inorg. Chem.*, **2006**, *14*, 2850-2584.

[19] Z. A. D. Lethbridge and P. Lightfoot, Mixed Inorganic Organic Anion Frameworks: Synthesis and Crystal Structure of $Fe_4(PO_4)_2(C_2O_4)(H_2O)_2$. *J. Solid State Chem.*, **1999**, *143*, 58-61.

[20] Z. A. D. Lethbridge, A. D. Hillier, R. Cywinski, P. Lightfoot, Mixed inorganic–organic anion frameworks: synthesis and characterisation of $[Mn_4(PO_4)_2(C_2O_4)(H_2O)_2]$ and $[H_3N(CH_2)_3NH_3][Mn_2(HPO_4)_2(C_2O_4)(H_2O)_2]$. *Dalton Trans.*, **2000**, 1595-1599.

[21] W. Yao, A. R. Armstrong and P. Lightfoot, A Novel Copper Oxalate, $Na_2Cu(C_2O_4)_2$. *Z. Anorg. Allg. Chem.*, **2016**, *642* (23), 1345-1349.

[22] W. Yao, M-T Sougrati, K. Hoang, J. N. Hui, P. Lightfoot and A. R. Armstrong. $Na_2Fe(C_2O_4)F_2$: A new iron-based polyoxyanion cathode for Li/Na ion batteries. *Chem. Mater.* **2017**, *29*, 2167-2172.

[23] J. H. Li, H. Liu, L. Wei and G. M. Wang, Two novel FeII-oxalate architectures: Solvent-free synthesis, structures, thermal and magnetic studies. *Solid State Sci.*, **2015**, *48*, 225-229.

[24] X. F. Wang, R. Kurono, S. Nishimura, M. Okubo and A. Yamada, Iron–Oxalato Framework with One-Dimensional Open Channels for Electrochemical Sodium-Ion Intercalation. *Chem. Eur. J.* **2015**, *21*, 1096-1101.

[25] X. Yang, J. Li, Y. W. Hou, S. Y. Shi and Y. K. Shan, $K_2Fe(C_2O_4)(HPO_4)(OH_2)H_2O$: A layered oxalatophosphate hybrid material. *Inorganica Chimica Acta*, **2008**, *361*, 1510-1514.

[26] E. Lhotel, V. Simonet, J. Ortloff, B. Canals, C. Paulsen, E. Suard, T. Hansen, D.J. Price, P.T. Wood, A.K. Powell and R. Ballou, Magnetic properties of a family of quinternary oxalates. *Eur. Phys. J. B.* **2013**, *86*, 248.

Table of Contents (TOC)